**Supporting Information for**

# Flexible Hierarchical Nanocomposites Based on $MnO_2$ Nanowires/CoAl Hydrotalcites/Carbon Fibers for High-Performance Supercapacitors

**Jingwen Zhao, Zhenzhi Lu, Mingfei Shao, Dongpeng Yan, Min Wei,* David G. Evans, and Xue Duan**

*State Key Laboratory of Chemical Resource Engineering, Beijing University of Chemical Technology, Beijing 100029, China*

* Corresponding author. Tel: +86-10-64412131; Fax: +86-10-64425385.

E-mail address: weimin@mail.buct.edu.cn (Min Wei).

## Experimental Section:

**Synthesis:** The $MnO_2$/LDH/CFs composite was prepared by a simple two-step process, which can be easily scaled up. First, the CoAl-LDH nanowalls material was synthesized using a solvothermal growth process on carbon fibers (CFs) substrate. In detail, $Co(NO_3)_2 \cdot 6H_2O$ (1 mmol), $Al(NO_3)_3 \cdot 9H_2O$ (0.5 mmol), $NH_4F$ (5 mmol) and urea (35 mmol) were dissolved in 50 mL of deionized water with $n$(Co)/$n$(Al)=2:1. The homogeneous solution was stirred thoroughly for 30 min and then transferred into a Teflon-lined stainless steel autoclave. CFs substrate was pretreated with concentrated $HNO_3$ solution and then cleaned in turn in an ultrasonic bath containing deionized water, acetone, ethanol and deionized water for 10 min each. Subsequently, the CFs substrate was immersed into the above solution at 90 °C for 6 h. The substrate coated with LDH nanowalls (LDH/CFs) was then withdrawn from the solution, washed extensively

with distilled water and dried at room temperature. The mass loading of LDH on CFs was 1.1 mg $cm^{-2}$. Second, the synthesis of $MnO_2$/LDH/CFs was carried out by simply soaking the above LDH/CFs in a solution containing 0.1 M $Na_2SO_4$ (Sigma-Aldrich) and 0.1 M $KMnO_4$ (Sigma-Aldrich) at ambient temperature for different time. The loading amount of $MnO_2$ can be easily controlled by prolonging the deposition time (Figure S3). Finally, the resulting $MnO_2$/LDH/CFs material was washed thoroughly with water to remove the remaining reagents and dried at ambient temperature. In addition, the control sample of $MnO_2$/CFs composite was obtained by direct electrodeposition of $MnO_2$ onto CFs by a reported method.[1] The loading amount of $MnO_2$ was controlled by the electrodeposition time (~1.2 mg $cm^{-2}$).

**Material characterization:** X-ray diffraction (XRD) patterns were recorded by a Rigaku XRD-6000 diffractometer, using Cu-K$\alpha$ radiation (0.15418 nm) at 40 kV, 30 mA. The morphology was investigated using a scanning electron microscope (SEM; Zeiss SUPRA 55) with an accelerating voltage of 20 kV, combined with energy dispersive X-ray spectroscopy (EDX). Transmission electron microscopy (TEM) images were recorded with Philips Tecnai 20 and JEOL JEM-2010 HR-TEM. X-ray photoelectron spectroscopy (XPS) measurements were performed using an ESCALAB 250 instrument (Thermo Electron) with Al K$\alpha$ radiation. Raman measurements were carried out with 633 nm of excitation by using a confocal Raman microspectrometer (Renishaw, inVia-Reflex, 633 nm). Nitrogen adsorption/desorption isotherms were measured on a Quantachrome Autosorb-1CVP analyzer. All samples were outgassed at 100 °C for 6 h under vacuum before measurements were recorded. The specific surface areas were calculated using the Brunauer-Emmett-Teller (BET) method.

**Electrochemical measurement:** A CHI 660B electrochemical workstation (Shanghai Chenhua

Instrument Co., China) was utilized for electrochemical measurements. Cyclic voltammetry (CV) curves and galvanostatic charge-discharge tests were carried out using a classical three-electrode cell with a saturated Hg/HgO electrode as the reference, a platinum plate as the counter in 1.0 M LiOH (Figure S14). The CFs-supported nanocomposites acted directly as the working electrode. Cyclic voltammetry (CV) was performed in a potential range between −0.2 and 0.65 V at different scan rates. Galvanostatic (GV) charge/discharge curves were obtained by cycling the potential from −0.2 to 0.6 V at various current densities to evaluate the specific capacitance. The weight-specific capacitance [F $g^{-1}$] and current rate [A $g^{-1}$] were calculated based on the total mass of the active materials (LDH and $MnO_2$). Electrochemical impedance spectroscopy (EIS) measurements were performed by applying an AC voltage with 5 mV amplitude in a frequency range from 0.01 to 100 kHz.

## Supplementary Figures

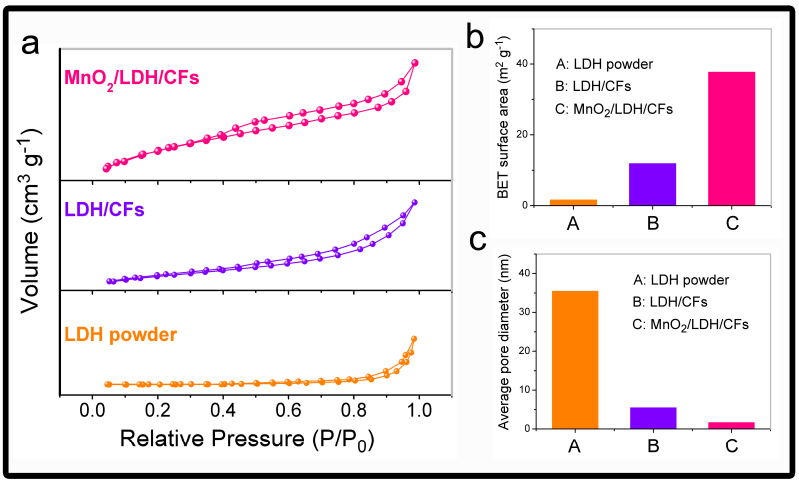


**Figure S1.** Gas adsorption/desorption analysis of $MnO_2$/LDH/CFs, LDH/CFs and LDH powdered sample: (a) nitrogen adsoption/desorption isotherms; (b) BET surface areas; (c) average pore diameters.

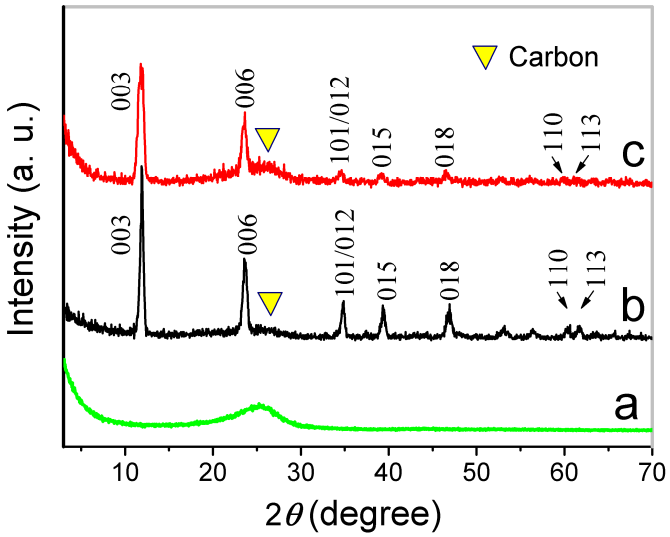


**Figure S2.** XRD patterns of (a) CFs, (b) LDH/CFs and (c) $MnO_2$/LDH/CFs.

The reflections of LDH/CFs (Figure S2, curve b) can be indexed to a hexagonal lattice with *R*3*m* rhombohedral symmetry, commonly used for the description of LDH structures. No other crystalline phase was detected, indicating the high purity of LDH grown on the conductive CFs. The XRD pattern of the $MnO_2$/LDH/CFs material (Figure S2, curve c) is very similar to that of the LDH/CFs one, indicating that the $MnO_2$ coating was amorphous. However, the redox reaction between $MnO_4^-$ and LDH induces a decrease in the crystallinity of LDH backbone, as displayed by the broadening of half-peak width for LDH reflections.

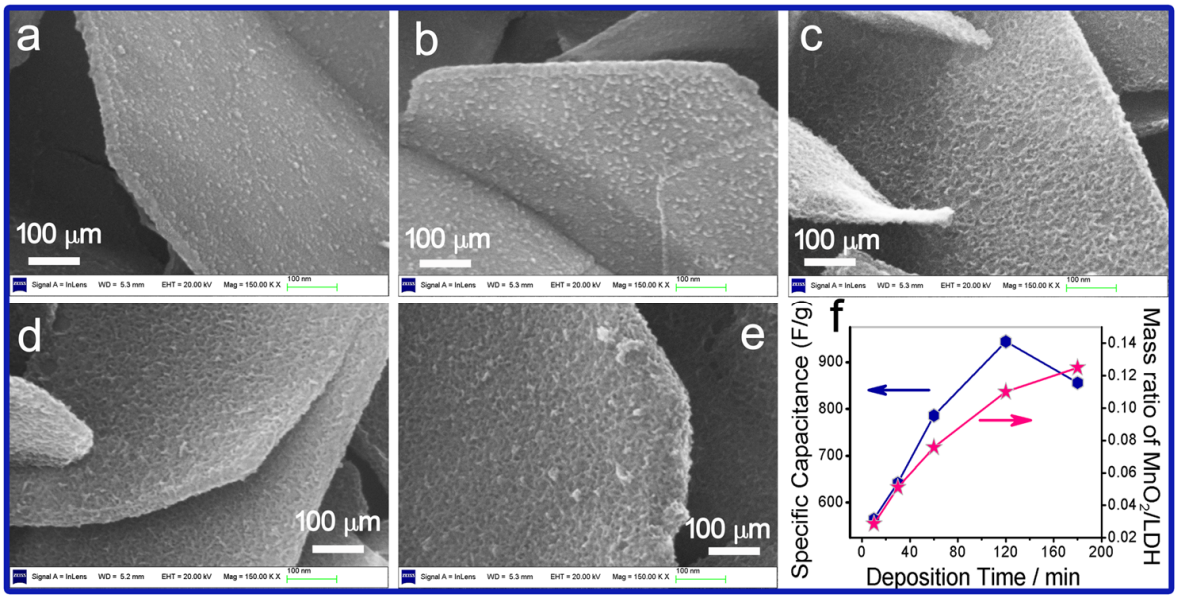


**Figure S3.** (a–e) SEM images of the $MnO_2$/LDH/CFs nanocomposite obtained with various deposition time of $MnO_2$: 10, 30, 60, 120 and 180 min, respectively; (f) specific capacitance and mass ratio of $MnO_2$/LDH as a function of deposition time, respectively.

Figure S3 shows that the $MnO_2$ nanowires gradually create a highly porous structure on the surface of LDH nanowalls with the increase of deposition time. Figure S3f reveals that the $MnO_2$/LDH/CFs sample with a deposition time of 120 min displays the highest specific capacitance (mass ratio of $MnO_2$/LDH is 0.11). By simply controlling the soaking time of the $KMnO_4$, we can regulate the loading amount of $MnO_2$. The results clearly illustrate the convenience of spontaneous redox deposition process in tailoring the morphological structure of the $MnO_2$/LDH/CFs composite.

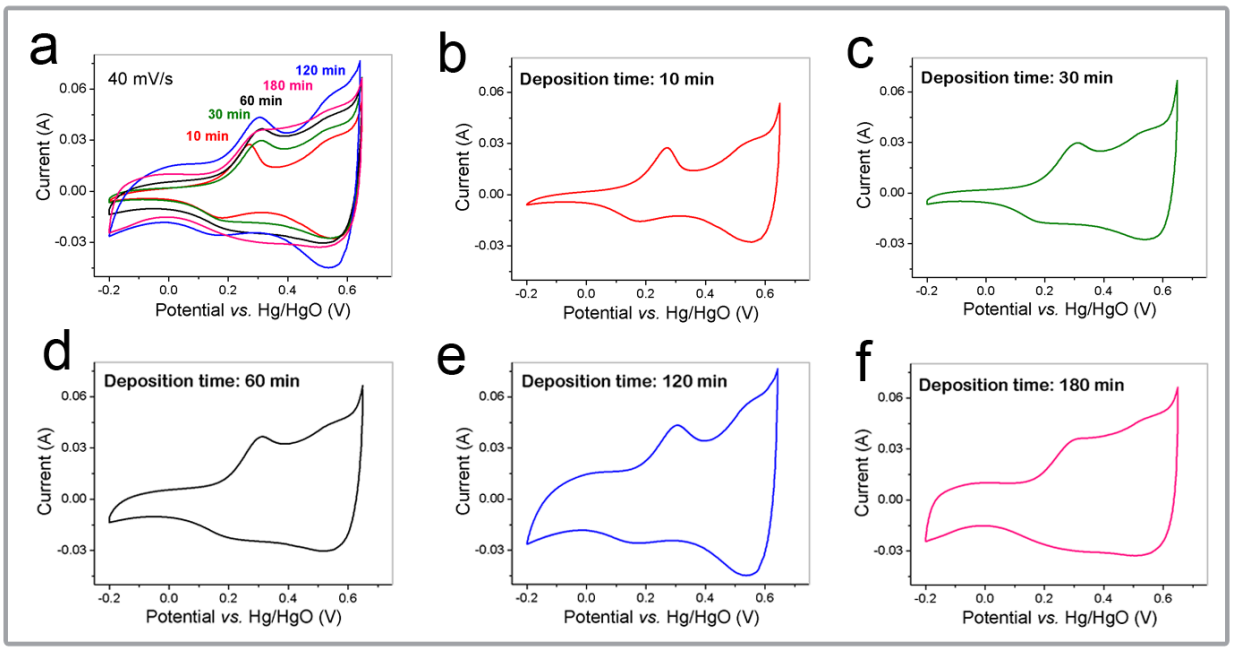


**Figure S4.** (a) Comparison of the CVs for the $MnO_2$/LDH/CFs electrodes obtained with various deposition time of $MnO_2$: 10, 30, 60, 120 and 180 min, respectively; (b–f) CVs of the $MnO_2$/LDH/CFs electrode as a function of deposition time.

Figure S4 shows the CVs of $MnO_2$/LDH/CFs electrodes as a function of deposition time at 40 mV $s^{-1}$. The current of $MnO_2$/LDH/CFs electrode increases with deposition time (10–120 min) due to the increase in $MnO_2$ loading on the LDH surface, which results in enhanced capacitance. However, a decrease in peak current was observed with further prolonging the deposition time to 180 min, as a result of the blocking effect of $MnO_2$ nanowires in a thick film.

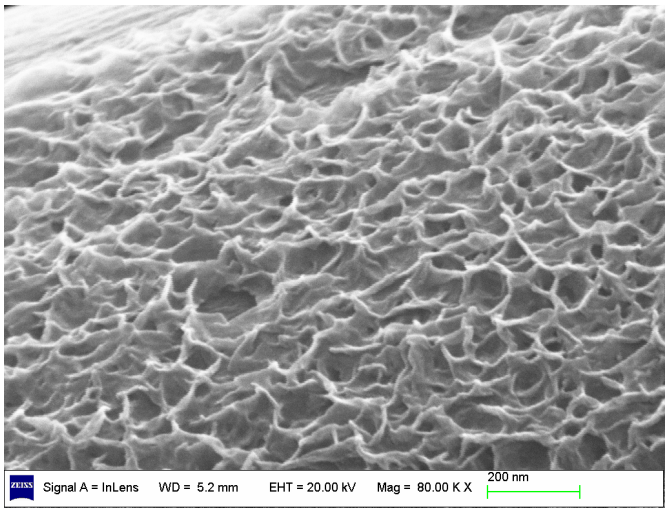


**Figure S5.** The SEM image of the $MnO_2$/CFs structure prepared by the electrodeposition method.

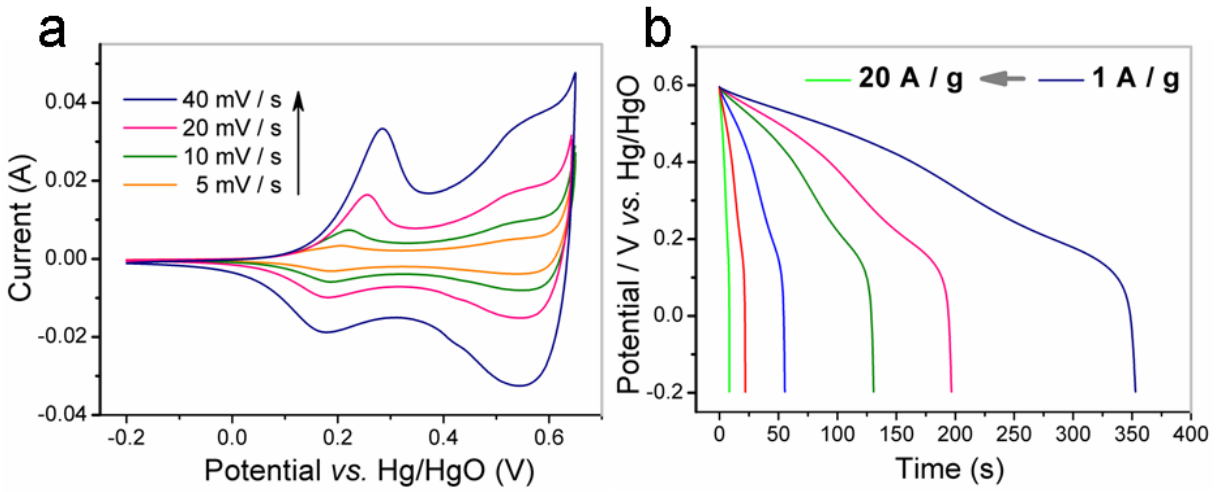


**Figure S6.** (a) CVs at different scan rates and (b) galvanostatic discharge curves at various discharge current densities of the LDH/CFs electrode.

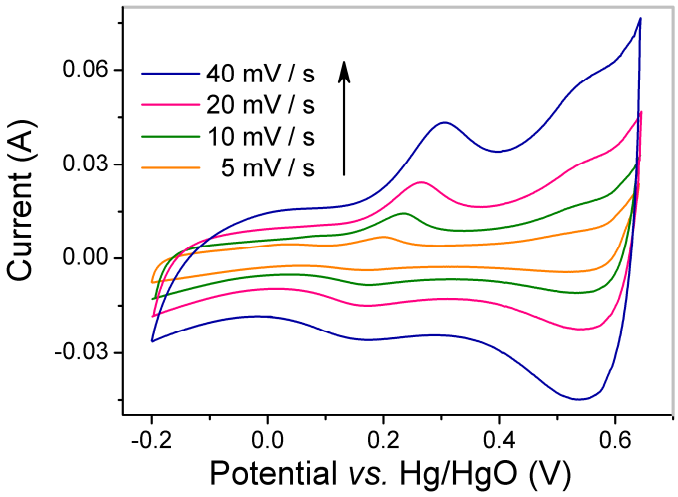


**Figure S7.** CVs of the $MnO_2$/LDH/CFs electrode with deposition time of 120 min at different scan rates: 5, 10, 20 and 40 mV $s^{-1}$, respectively.

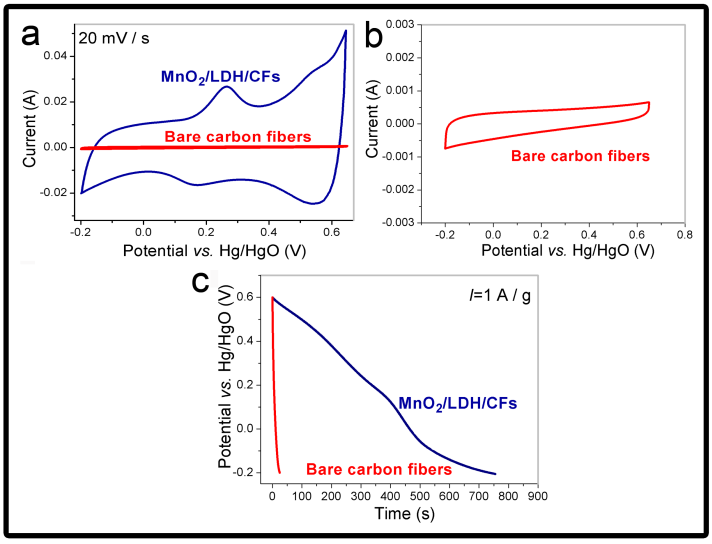


**Figure S8.** (a) CVs of the $MnO_2$/LDH/CFs and bare CFs (carbon fibers) at a scan rate of 20 mV $s^{-1}$; (b) enlarged view of CV for bare CFs; (c) Galvanostatic discharge curves for the $MnO_2$/LDH/CFs and bare CFs at a current density of 1 A $g^{-1}$, respectively.

The capacitance of pure CFs was calculated to be 31 F $g^{-1}$ at the current of 1 A $g^{-1}$ based on the galvanostatic charge/discharge curve. Clearly, the capacitance of $MnO_2$/LDH/CFs is ~30 times higher than that of bare CFs, indicating that CFs in this study deliver negligible capacitance.

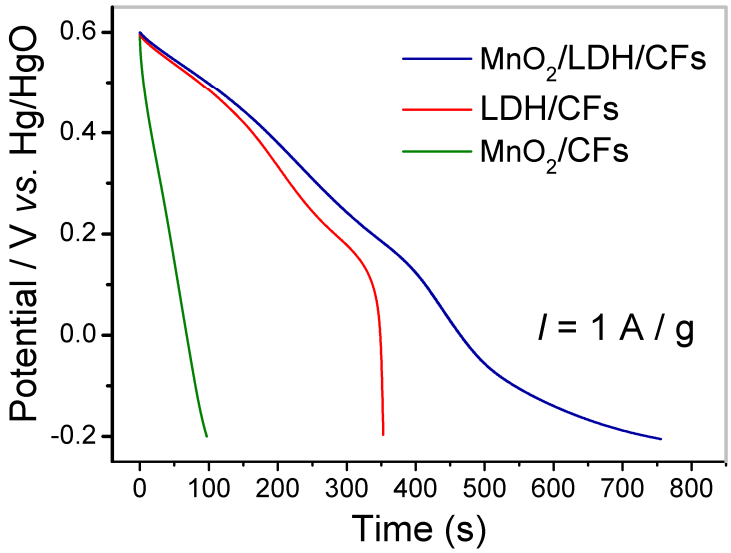


**Figure S9.** Galvanostatic discharge curves for the samples of $MnO_2$/LDH/CFs, LDH/CFs and $MnO_2$/CFs at a current density of 1 A $g^{-1}$.

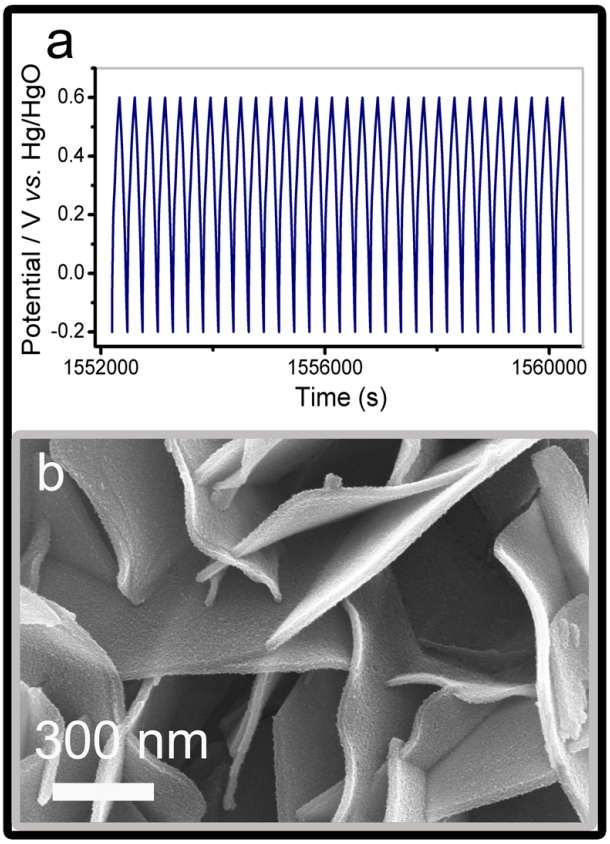


**Figure S10.** (a) The charge–discharge curves of the last 30 cycles and (b) a typical SEM image for the $MnO_2$/LDH/CFs electrode after 6000 cycles.

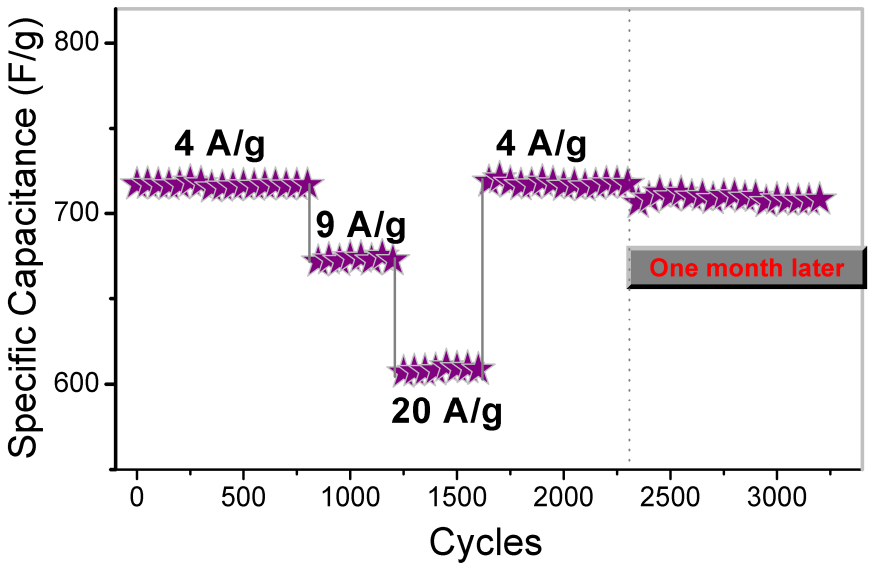


**Figure S11.** Cycling response of the $MnO_2$/LDH/CFs electrode at varying current densities.

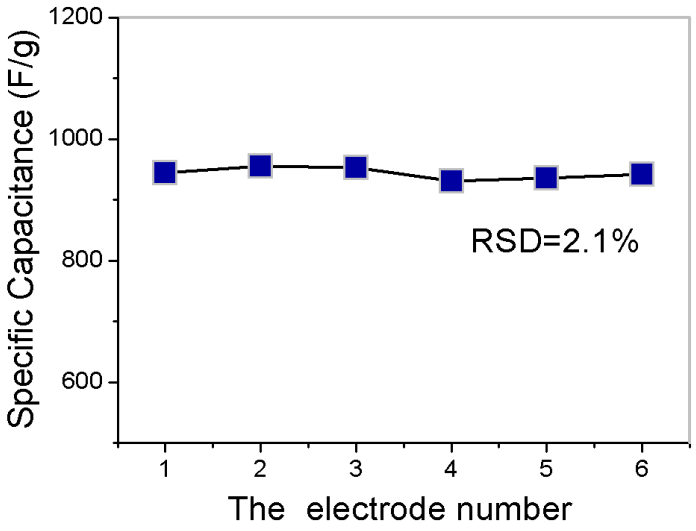


**Figure S12.** The reproducibility of the $MnO_2$/LDH/CFs electrode: specific capacitances of six parallel electrodes at the current density of 1 A $g^{-1}$.

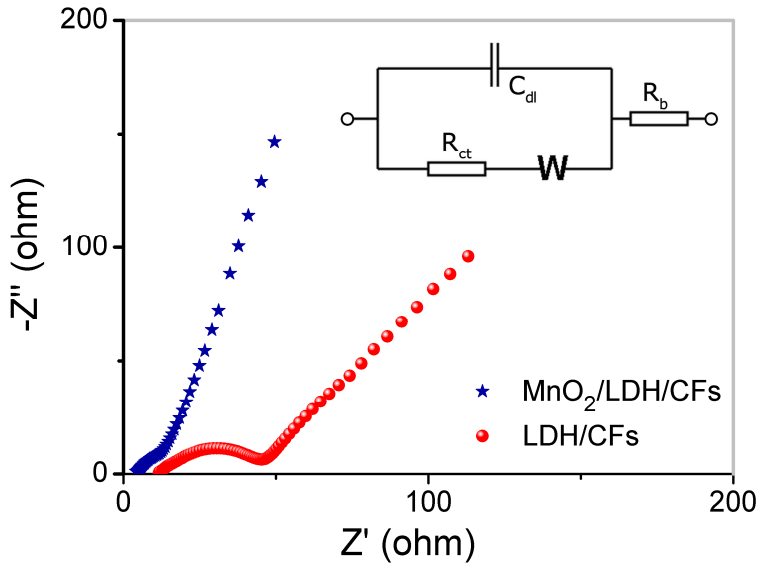


**Figure S13.** Impedance Nyquist plots of the $MnO_2$/LDH/CFs and LDH/CFs electrode, respectively (the inset shows the corresponding equivalent circuit model).

Figure S13 shows the Nyquist plots of the $MnO_2$/LDH/CFs and LDH/CFs electrode, respectively. The semicircle in high frequency regions reflects the electrochemical reaction impedance of the film electrode; the slope of the long tail at low frequency area shows the Warburg impedance (W) which represents the electrolyte diffusion in the porous electrode and proton diffusion in host materials.[2–4] The loading of the $MnO_2$ layer leads to a smaller diameter of the semicircle, indicating a lower charge-transfer resistance in the $MnO_2$/LDH/CFs electrode than that in the LDH/CFs one. Additionally, the $MnO_2$/LDH/CFs electrode displays a more ideal straight line along the imaginary axis, which demonstrates a lower diffusion resistance. This is due to the well-defined porous architecture of $MnO_2$ nanowires, making them fully available to the electrolyte.[5]

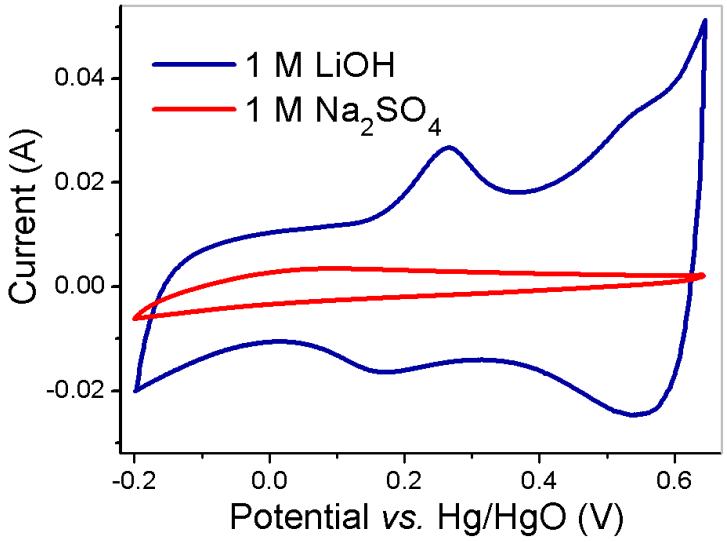


**Figure S14.** Comparison of CVs for the $MnO_2$/LDH/CFs electrode in LiOH and neutral $Na_2SO_4$ electrolyte at 20 mV $s^{-1}$. The significant increase in the CV integrated area and well-defined redox peaks indicate that LiOH is more suitable as electrolyte in this work.

## References

(1) N. Cherchour, C. Deslouis, B. Messaoudi and A. Pailleret, *Electrochim. Acta*, 2011, **56**, 9746.

(2) R. B. Rakhi, W. Chen, D. Cha and H. N. Alshareef, *Nano Lett.*, 2012, **12**, 2559.

(3) X. Li, J. Rong and B. Wei, *ACS Nano*, 2010, **10**, 6039.

(4) B. Ballarin, M. C. Cassani, E. Scavetta and D. Tonelli, *Electrochim. Acta*, 2008, **53**, 8034.

(5) J. Liu, J. Jiang, C. Cheng, H. Li, J. Zhang, H. Gong and H. J. Fan, *Adv. Mater.*, 2011, **23**, 2076.